(This is a sample cover image for this issue. The actual cover is not yet available at this time.)

Earth and Planetary Science Letters 361 (2013) 134–142

Contents lists available at SciVerse ScienceDirect

Earth and Planetary Science Letters

journal homepage: www.elsevier.com/locate/epsl

Elasticity of single-crystal iron-bearing pyrope up to 20 GPa and 750 K

Chang Lu [a,*], Zhu Mao [a], Jung-Fu Lin [a], Kirill K. Zhuravlev [b], Sergey N. Tkachev [b], Vitali B. Prakapenka [b]

[a] Department of Geological Sciences, Jackson School of Geosciences, The University of Texas at Austin, Austin, TX 78712, USA
[b] Center for Advanced Radiation Sources, University of Chicago, Chicago, IL 60637, USA

ARTICLE INFO

Article history:
Received 9 July 2012
Received in revised form
7 November 2012
Accepted 19 November 2012
Editor: L. Stixrude

Keywords:
single-crystal elasticity
Fe-bearing pyrope
high pressure–temperature
Brillouin scattering
upper mantle

ABSTRACT

Elastic properties of the major constituent minerals in the Earth's upper mantle at relevant high pressure–temperature (P–T) conditions are crucial for understanding the composition and seismic velocity structures of this region. In this study, for the first time, we have measured the single-crystal elasticity of natural Fe-bearing pyrope, $Mg_{2.04}Fe_{0.74}Ca_{0.16}Mn_{0.05}Al_2Si_3O_{12}$, using *in situ* Brillouin spectroscopy and X-ray diffraction at simultaneous high P–T conditions up to 20 GPa and 750 K in an externally-heated diamond anvil cell. The derived aggregate adiabatic bulk and shear moduli (K_{S0}, G_0) at ambient conditions are 168.2 ($\pm$1.8) GPa (the value in parentheses represents propagated uncertainties $\pm 1\sigma$) and 92.1 ($\pm$1.1) GPa, respectively, consistent with literature results. Using the third-order Eulerian finite-strain equation to model the high P–T data, the derived pressure derivatives of the bulk and shear moduli at constant temperature are $(\partial K_S/\partial P)_T$=4.4 ($\pm$0.1) and $(\partial G/\partial P)_T$=1.2 ($\pm$0.1), respectively, whereas the temperature derivatives of these moduli at constant pressure are $(\partial K_S/\partial T)_P$=−16.8 ($\pm$1.3) MPa/K and $(\partial G/\partial T)_P$=−5.1 ($\pm$1.1) MPa/K, respectively. Compared to literature values, our results show that addition of 25 mol% Fe in pyrope increases the pressure derivative of the bulk modulus by 7%, but has a negligible effect on other elastic parameters. Extrapolation of our results shows that Fe-bearing pyrope remains almost elastically isotropic at relevant P–T conditions of the upper mantle, indicating that it may not have a significant contribution to seismic V_P and V_S anisotropy in the upper mantle. Together with the elasticity of olivine and pyroxene minerals in the upper mantle, we have constructed new velocity profiles for two representative compositional models, pyrolite and piclogite, along a representative geotherm of the Earth's upper mantle. These velocity models show V_S profiles consistent with seismic observations, although V_P profiles are slightly lower than global seismic observations. Our analyses also show that approximately 30% garnet in a mineralogical model is needed to best match both seismic V_P and V_S profiles of the region, although such high garnet content needs to be reconciled with our current geochemical understanding. Our results here provide new insights into seismic profiles and mineralogical models of the upper mantle region.

1. Introduction

Iron-bearing pyrope is an abundant mineral in the Earth's upper mantle. According to the pyrolitic compositional model, Earth's upper mantle (e.g. up to approximately 410 km depth) is mainly composed of ~63% olivine, ~22% pyroxene, and ~15% garnet by volume (Ringwood, 1975; Ita and Stixrude, 1992). With increasing depth, the volume fraction of garnet could increase to 40% or more because pyroxene is expected to dissolve into garnet and transform into majoritic garnet solid solution starting at the base of the upper mantle (Ringwood, 1967, 1991; Ita and Stixrude, 1992; Fei and Bertka, 1999). Due to its stability in the transition zone, majoritic garnet is one of the most abundant minerals in that region. Garnet is also abundantly present in the mineral assemblage of eclogites formed from high-pressure mafic rocks (Poli, 1993). Upper-mantle garnet is mainly composed of pyrope ($Mg_3Al_2Si_3O_{12}$), with ~6–23% iron and ~2–15% calcium substituting for magnesium (Rickwood et al., 1968; Sinogeikin and Bass, 2002; Lee, 2003). The presence of Fe^{2+} and Ca^{2+} in the system has been known to affect a number of physical properties of pyrope, including elasticity (e.g. Verma, 1960; Sumino and Nishizawa, 1978; Suzuki and Anderson, 1983), electrical conductivity (e.g. Romano et al., 2006; Dai and Karato, 2009), and thermal conductivity (e.g. Kanamori et al., 1968; Giesting and Hofmeister, 2002).

Considering the abundance of garnet in the Earth's upper mantle and transition zone, experimental studies on the elasticity of iron-bearing pyrope with a relevant composition at upper-

* Corresponding author.
E-mail address: lcer.jsg@utexas.edu (C. Lu).

0012-821X/$ - see front matter © 2012 Elsevier B.V. All rights reserved.
http://dx.doi.org/10.1016/j.epsl.2012.11.041

mantle P–T conditions have significant implications for constraining seismic observations and for understanding the chemical composition of the deep Earth (e.g. Bass and Anderson, 1984; Duffy and Anderson, 1989; Cammarano et al., 2003; Li and Liebermann, 2007). There have been a number of previous measurements on the elasticity of pyrope-rich garnet at high pressures and room temperature (e.g. Chen et al., 1999; Conrad et al., 1999; Sinogeikin and Bass, 2000) or at room pressure and high temperatures (e.g. Sumino and Nishizawa, 1978; Suzuki and Anderson, 1983; Sinogeikin and Bass, 2002). Additionally, ultrasonic measurements on the sound velocities of polycrystalline Mg-end member pyrope have been reported up to 9 GPa and 1300 K (Gwanmesia et al., 2006, 2007), yet laboratory measurements on the single-crystal elasticity of iron-bearing pyrope at relevant chemical and P–T conditions of the upper mantle remain lacking.

In the upper mantle, seismological studies have revealed the existence of global azimuthal anisotropies (e.g. Hess, 1964; Raitt et al., 1969), shear wave (V_S) polarization anisotropies (e.g. Ando et al., 1980; Montagner and Tanimoto, 1990) and their regional variations (e.g. Silver and Chan, 1991). Montagner and Kennett (1996) have reported shear wave and compressional wave anisotropies of the upper mantle, $\xi=(V_{SH}/V_{SV})^2$ and $\varphi=(V_{PV}/V_{PH})^2$, where the subscript H represents the seismic wave velocity in the horizontal direction, and the subscript V represents the vertical direction in several global seismic models. In the AK135-f Earth model (Kennett, 1991; Kennett et al., 1995), for example, ξ decreases from $\sim$1.06 to 1 with increasing depth from the surface to 400 km depth in the upper mantle, while φ increases from $\sim$0.94 to 1. It has been proposed that the observed seismic anisotropy is a result of the lattice-preferred orientation and elastic anisotropies of major minerals in the upper mantle (e.g. Kawasaki and Konno, 1984; Mainprice et al., 2000). Understanding and interpreting the observed seismic anisotropy thus requires detailed knowledge of the single-crystal elasticity of the constituent minerals in the upper mantle.

In this study, for the first time, we have measured the single-crystal elasticity of iron-bearing pyrope with 25 mol% Fe up to 20 GPa and 750 K using *in situ* Brillouin spectroscopy and X-ray diffraction in an externally-heated diamond anvil cell (EHDAC). We have evaluated high P–T and iron compositional effects on the sound velocities of garnet as well as its V_P and V_S anisotropies to aid our current understanding of seismic velocity and mineralogical models of the upper mantle.

2. Experimental details

Natural single crystals of Fe-bearing pyrope, $(Mg_{2.04}Fe_{0.74}Ca_{0.16}Mn_{0.05})Al_2Si_3O_{12}$, from East Africa were analyzed for chemical composition by electron microprobe (JEOL 8200) and lattice parameters by X-ray diffraction. These analyses showed that the samples, with a lattice parameter $a=11.5041$ ($\pm$0.0021) Å (cubic system), were chemically homogeneous with 24.7 ($\pm$0.1) mol% Fe, 5.3 ($\pm$0.1) mol% Ca, and 1.7 ($\pm$0.1) mol% Mn. The orientation of the sample platelets was determined by single-crystal X-ray diffraction (XRD) at the Texas Materials Institute of the University of Texas at Austin (UT-Austin) and the GSECARS sector of the Advanced Photon Source (APS), Argonne National Laboratory (ANL). Sample platelets were doubled-side polished down to approximately 15–35 μm thick in (110) crystallographic orientation or in an orientation close to (−0.21, 0.92, 0.34), which was randomly selected from polished platelets. The use of the (110) platelets permits determination of the elastic constants (C_{11}, C_{12}, C_{44}) along principal ⟨100⟩, ⟨110⟩ and ⟨111⟩ axes based on the following equations:

$$\rho V^2_{P\langle 100\rangle} = C_{11} \tag{1}$$

$$\rho V^2_{S\langle 100\rangle} = C_{44} \tag{2}$$

$$\rho V^2_{P\langle 110\rangle} = (C_{11}+2C_{44}+C_{12})/2 \tag{3}$$

$$\rho V^2_{S\langle 111\rangle} = (C_{11}+C_{44}-C_{12})/3 \tag{4}$$

where the subscript ⟨uvw⟩ indicates the symmetry family of directions corresponding to the scattering wave vector, and ρ indicates the density. The platelet with the general (or non-special) orientation was used for further confirmation of the measured elasticity. A cylindrical hole of 220 μm in diameter was drilled in 50–60 μm thick pre-indented Re gaskets and used as the sample chamber. A single-crystal platelet was loaded into the sample chamber of an EHDAC which had Pt wires as the external resistive heating element (Mao et al., 2012). In total, seven separate platelets were used in the experiments for high P–T Brillouin and/or XRD experiments. Ne was loaded in the chamber as the pressure medium for all experiments. Au powder was loaded close to the sample as the pressure calibrant (Fei et al., 2007), and ruby spheres next to the sample were used as a pressure scale at high pressures and room temperature (Mao et al., 1986). A K-type thermocouple was attached to the diamond surface approximately 500 μm away from the diamond culet for temperature measurements.

High P–T Brillouin measurements were performed at GSECARS of APS, ANL up to 20 GPa with temperatures of 300, 500, and 750 K (Sinogeikin et al., 2006). The temperature was kept below 750 K to avoid potential oxidation and failure of diamonds and heaters from resistive heating. A series of XRD patterns of the Au pressure calibrant were collected for pressure determinations at high P–T to ensure the pressure stability of the experiments. Brillouin measurements were only conducted when no significant shift in pressure determined from the XRD patterns was observed. These XRD patterns of pyrope were also used to determine the density of the sample at high P–T conditions. High-pressure Brillouin measurements at 300 K were also conducted at the Mineral Physics Laboratory of UT-Austin using the newly built Brillouin spectroscopic system. The Brillouin setup at UT-Austin is equipped with a Coherent Verdi 532 nm laser, a photomultiplier tube (PMT) which provides a low dark count rate (<2 counts/s), and a JRS six-pass tandem Fabry–Perot Interferometer. The laser beam can be focused to approximately 20 μm beam diameter at the sample position. The scattering angle has been set to 50° and calibrated using previously reported elastic constants of silicate glass (Polian et al., 2002), distilled water (Ostwald et al., 1977) and single-crystal MgO calibrants (Sinogeikin and Bass, 2000). XRD patterns of the sample were also collected at the High-Pressure Collaborative Access Team (HPCAT) sector of APS, ANL to evaluate the pressure–density equation of state (EoS) of the sample at 300 K (Birch, 1978).

3. Results

High P–T Brillouin and XRD spectra were collected up to 20 GPa and 750 K. Most of the Brillouin spectra showed strong V_P and V_S peaks with high signal-to-noise ratios except for some crystallographic directions where V_P peaks were weakly observable. Although two polarized V_S peaks were expected to exist, only one V_S peak was observed in our study, likely a result of two overlapping V_S peaks due to the small anisotropy (Fig. 1). The

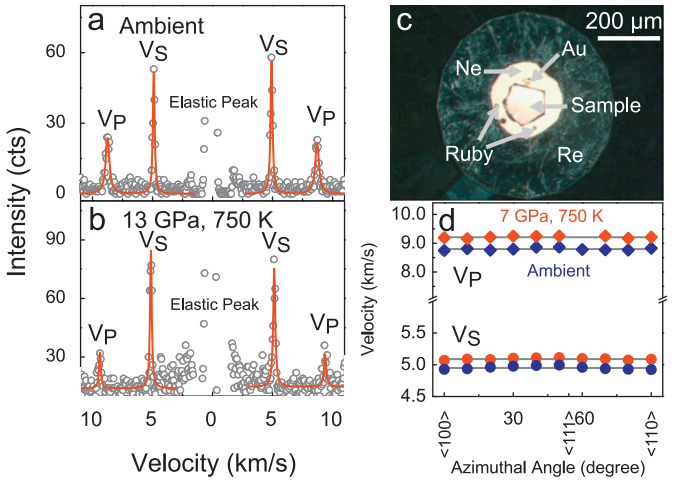

Fig. 1. Representative Brillouin spectra of Fe-bearing pyrope. (a) Ambient conditions; (b) 13 GPa and 750 K; (c) photomicrograph of the sample chamber in an EHDAC after gas loading; (d) V_P and V_S velocities of the Fe-bearing pyrope as a function of the azimuthal angle from a (110) platelet. Blue symbols: ambient conditions; red symbols: 7 GPa and 750 K; solid lines: modeled results (Eq. (5)). Error bars are smaller than the symbols when not shown. Crystallographic directions ⟨100⟩, ⟨111⟩ and ⟨110⟩ are labeled for clarity. (For interpretation of the references to color in this figure legend, the reader is referred to the web version of this article.)

variation in V_P and V_S as a function of the azimuthal angle was not observed outside experimental uncertainties (Fig. 1). Both V_P and V_S peaks of the Ne medium were also observed at pressures below ~8 GPa, but they were not as visible when pressure increased. Analysis of the results for the elastic constants from the pre-oriented (110) platelets and from general orientation platelets show that V_P and V_S are consistent within experimental uncertainties (Fig. 2).

Single-crystal elastic constants (C_{ij}) of the sample were obtained by fitting the measured spatial dispersion (velocity vs. orientation) of acoustic V_P and V_S velocities to Christoffel's equation using non-linear least squares methods (Fig. 2) (Every, 1980):

$$|C_{ijkl}n_jn_l-\rho V^2\delta_{ik}|=0 \tag{5}$$

where C_{ijkl} are the elastic constants in full four-indices notation, which can be simplified using reduced Voigt notation C_{ij}. n_i is the direction cosines of the phonon propagation direction and is described by three Eulerian angles (θ, χ, φ), V is the measured acoustic velocity, and δ_{ik} is the Kronecker delta. As shown in previous studies (e.g. Sinogeikin and Bass, 2000), the elastic constants of pyrope can be obtained by averaging the measured acoustic velocities over several non-symmetric directions, because pyrope is nearly elastically isotropic up to 20 GPa at 300 K. We note that the elastic constants of Fe-bearing pyrope obtained from the least-squares fitting to the Christoffel's equation are indistinguishable within experimental uncertainties from those derived from averaging the measured velocity assuming isotropic elastic constants (Table 1).

Using the derived elastic constants of the sample, we have calculated the aggregate adiabatic bulk and shear moduli (K_S and G) using the Voigt–Ruess–Hill averages (Hill, 1952):

$$K_S=C_{11}-2C/3 \tag{6}$$

$$G=[(C/5+3C_{44}/5)+5C_{44}C/(4C_{44}+3C)]/2 \tag{7}$$

$$C=C_{11}-C_{12} \tag{8}$$

Table 1
Single-crystal elastic moduli of the Fe-bearing pyrope values from two different models (fitted and averaged) are listed for comparison.

	1 bar, 300 K		20 GPa, 750 K	
	Fitted[a] C_{ij}	Averaged[b] C_{ij}	Fitted[a] C_{ij}	Averaged[b] C_{ij}
C_{11} (GPa)	290.4 (±1.8)	290.9 (±3.3)	393.3 (±2.4)	395.1 (±4.0)
C_{12} (GPa)	106.2 (±2.0)	106.8 (±1.1)	170.9 (±2.4)	171.4 (±1.4)
C_{44} (GPa)	92.2 (±0.6)	92.1 (±1.1)	112.1 (±1.0)	111.9 (±1.3)
K_s (GPa)	168.5 (±1.9)	168.2 (±1.8)	245.0 (±2.0)	246.0 (±2.3)
G (GPa)	91.9 (±1.1)	92.1 (±1.1)	111.5 (±0.3)	111.9 (±1.3)

[a] Fitted C_{ij}: C_{ij} were obtained from fitting the measured velocity to the Christoffels' equation.
[b] Averaged C_{ij}: C_{ij} were obtained from averaging the measured velocity assuming elastic isotropy of Fe-bearing pyrope.

The derived K_{S0} and G_0 at ambient conditions are 168.2 (±1.8) GPa and 92.1 (±1.1) GPa, respectively. The pressure derivatives of the elastic moduli at 300 K were obtained by fitting the moduli at high pressure using the third-order Eulerian finite-strain equation (Birch, 1978):

$$K_S=K_{S0}(1+2f)^{5/2}\{1+[3(\partial K_S/\partial P)_T-5]f\} \tag{9}$$

$$G=(1+2f)^{5/2}\{G_0+[3(\partial G/\partial P)_TK_{S0}-5G_0]f\} \tag{10}$$

$$f=(1/2)[(\rho/\rho_0)^{2/3}-1] \tag{11}$$

where $(\partial K_S/\partial P)_T$ and $(\partial G/\partial P)_T$ are the pressure derivatives of the bulk and shear moduli, respectively, at constant temperature, f is the normalized strain, ρ is density at a given pressure, and ρ_0 is the density at ambient conditions. Considering the well-known tradeoff between K_{T0} and $(\partial K_T/\partial P)_T$ in third order Birch–Murnaghan EoS fitting, we have adopted the following procedures to ensure the robustness of our fitting results. Thermal EoS parameters from the literature were first used for calculating the density values for the initial finite-strain fitting (Sinogeikin and Bass, 2000). Once $(\partial K_S/\partial P)_T$ was obtained from the modeling, the K_S and $(\partial K_S/\partial P)_T$ were converted to the isothermal K_T and $(\partial K_T/\partial P)_T$ using the following thermodynamic relations (Jiang et al., 2004):

$$K_{T0}=K_{S0}/(1+\alpha\gamma T) \tag{12}$$

$$(\partial K_T/\partial P)_T\approx(1+\alpha\gamma T)^{-1}[(\partial K_S/\partial P)_T-(\gamma T/K_{T0})(\partial K_T/\partial T)_P] \tag{13}$$

where $(\partial K_T/\partial T)_P$ is the temperature derivative of K_T at constant pressure, α is the volume thermal expansion coefficient (Fei, 1995), and γ is the Grüneisen parameter (Gillet et al., 1992). The pressure–density curve at 300 K from our single-crystal X-ray diffraction study was also fitted to the third-order Birch–Murnaghan EoS (Birch, 1978) using a fixed $(\partial K_T/\partial P)_T$ from Eq. (13):

$$P=3K_{T0}f(1+2f)^{5/2}\{1+(3/2)[(\partial K_T/\partial P)_T-4]f\} \tag{14}$$

Differences in K_T using Eqs. (12) and (14) were further used to improve the trial density values. These aforementioned procedures were repeated until both K_T and $(\partial K_T/\partial P)_T$ were self-consistent with satisfactory density values. With the thermal EoS values determined, the pressure derivatives of the three elastic constants and the bulk and shear moduli were derived to be: $(\partial C_{11}/\partial P)_T$=6.0 (±0.1), $(\partial C_{12}/\partial P)_T$=3.5 (±0.1), $(\partial C_{44}/\partial P)_T$=1.2 (±0.1), $(\partial K_S/\partial P)_T$=4.4 (±0.1), and $(\partial G/\partial P)_T$=1.2 (±0.1) (Table 2), using the third-order Eulerian finite-strain equations (Birch, 1978).

Due to limited data points at high temperature, a linear equation was applied to obtain the temperature derivatives of the elastic moduli at high pressures to evaluate the temperature effect under high pressure (Gwanmesia et al., 2006, 2007; Irifune

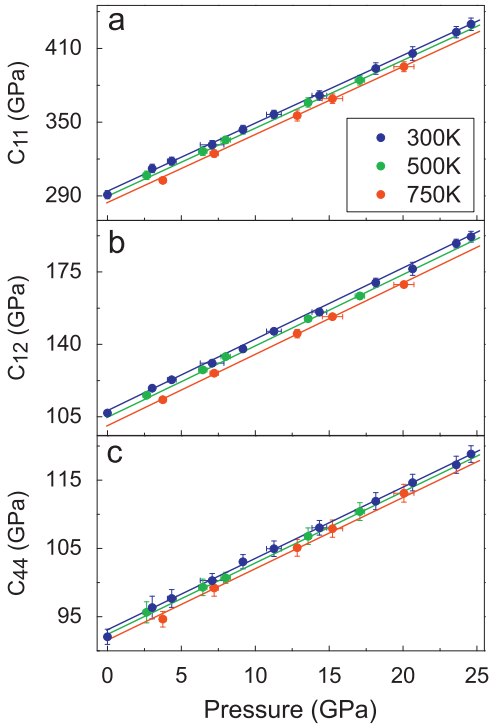

Fig. 2. Single-crystal elastic constants of the Fe-bearing pyrope at high P–T from (110) and random orientation platelets. Blue, green and red circles: experimental values at 300 K, 500 K and 750 K, respectively; blue, green and red solid lines: modeled results at 300 K, 500 K and 750 K from linear fitting, respectively (see Eq. (15) for details). (For interpretation of the references to color in this figure legend, the reader is referred to the web version of this article.)

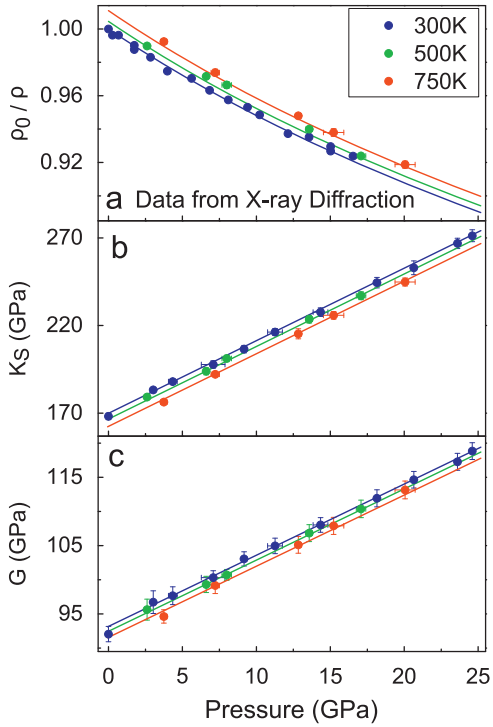

Fig. 3. Equation of state and aggregate bulk and shear moduli of the Fe-bearing pyrope. (a) Pressure–density relation of Fe-bearing pyrope; (b) adiabatic bulk modulus (K_S); (c) shear modulus (G). Blue, green and red circles: experimental data at 300 K, 500 K and 750 K, respectively. A third-order Birch–Murnaghan equation of state was applied to fit the data from high P–T (300 K, 500 K and 750 K) X-ray diffraction, whereas K_S and G were analyzed using the linear fitting (blue, green and red solid lines) (see Eqs. (14) and (15)). (For interpretation of the references to color in this figure legend, the reader is referred to the web version of this article.)

et al., 2008):

$$M = M_0 + (P-P_0)(\partial M/\partial P)_T + (T-T_0)(\partial M/\partial T)_P \quad (15)$$

where M is either the C_{ij} or the elastic moduli (K_S and G), and P_0 and T_0 are ambient pressure and temperature, respectively. The temperature derivatives of the elastic constants and moduli are: $(\partial C_{11}/\partial T)_P = -20.5$ (± 4.0) MPa/K, $(\partial C_{12}/\partial T)_P = -16.3$ (± 0.5) MPa/K, $(\partial C_{44}/\partial T)_P = -3.4$ (± 1.4) MPa/K, $(\partial K_S/\partial T)_P = -16.5$ (± 2.0) MPa/K and $(\partial G/\partial T)_P = -3.6$ (± 1.4) MPa/K (Figs. 2 and 3 and Tables 2 and 3). We note that the second-order derivatives of the elastic moduli such as $\partial^2 K_S/(\partial P \partial T)$ and $\partial^2 G/(\partial P \partial T)$ of pyrope, which represent the coupling effects of P and T on K_S and G, are expected to be very small (in the order of 10^{-4} K^{-1}) (Gwanmesia et al., 2007) and are neglected in our model. The temperature derivatives of the elastic moduli were also evaluated with fixed K_{S0} and $(\partial K_S/\partial P)_T$ values from room temperature study in the linear fitting procedure (see Eq. (15)), because the M_0 and $(\partial M/\partial P)_T$ values are better constrained at room temperature with more experimental data points. These combined procedures are referred to as the revised linear fitting method in the discussion below (Tables 2 and 3).

4. Discussion

4.1. The effect of iron on the elasticity of pyrope at high P–T

In order to understand the effect of Fe on the elasticity of the pyrope–almandine joint, we have compared our results to literature values obtained from Brillouin scattering and ultrasonic interferometer measurements (Figs. 4 and 5 and Table 2) (Verma, 1960; Soga, 1967; Bonczar et al., 1977; Leitner et al., 1980; Webb, 1989; O'Neill et al., 1991; Chen et al., 1997, 1999; Conrad et al., 1999; Sinogeikin and Bass, 2000; Wang and Ji, 2001; Jiang et al., 2004; Gwanmesia et al., 2006, 2007). Here the potential effect of Ca and Mn on the elasticity of pyrope is not considered because of their limited amounts in the studied samples. At ambient conditions, comparative analysis of these results show that addition of Fe does not show a visible effect on the K_S, G and $(\partial G/\partial P)_T$ of pyrope within experimental uncertainties, although increasing the Fe content in pyrope appears to have a weak positive effect on the $(\partial K_S/\partial P)_T$ in results obtained from the same Brillouin technique (Fig. 4). Specifically, our derived $(\partial K_S/\partial P)_T$ for pyrope with 25 mol% Fe is ~7% greater than that of pure pyrope (Sinogeikin and Bass, 2000), but ~6% lower than that with 72 mol% Fe (Jiang et al., 2004).

Due to the well-known tradeoff between the derived elastic modulus and its pressure derivative values in EoS fittings, we have plotted the K_s and G of three representative compositions in pyrope–almandine system at high pressures using Brillouin scattering results (Fig. 5). Comparison of pure pyrope and our results shows that adding 25 mol% Fe to pyrope does not affect the bulk modulus but may slightly reduce the shear modulus at high pressures, while a previous study on pyrope with 72 mol% Fe by Jiang et al. (2004) shows that adding Fe will increase both bulk and shear modulus. Jacobsen et al. (2002) have reported that the Fe effect on elasticity in some single-crystal minerals may not be a simple linear function. In their study, adding Fe to MgO can increase its adiabatic bulk modulus up to ~10 mol% of FeO, but (Mg,Fe)O with more than ~60 mol% FeO has a lower bulk modulus than its pure MgO counterpart. Systematic studies on the pyrope–almandine samples using similar experimental techniques and conditions are needed in the future to further clarify

Table 2
Bulk and shear moduli and their pressure derivatives of the pyrope–almandine garnets.[a]

Study	P_{max} (GPa)	Composition[b]	K_{S0} (GPa)	$(\partial K_S/\partial P)_T$	G_0 (GPa)	$(\partial G/\partial P)_T$
Brillouin scattering						
This study (revised)	24.6	Py68Alm24Gr5Sp1	168.2 (±1.8)	4.4 (±0.1)	92.1 (±1.1)	1.2 (±0.1)
This study (linear)	24.6	Py68Alm24Gr5Sp1	169.9 (±0.7)	4.1 (±0.1)	93.2 (±0.6)	1.0 (±0.1)
Sinogeikin and Bass (2000)	20	Py100	171.2 (±2.0)	4.1 (±0.3)	93.7 (±2.0)	1.3 (±0.2)
Conrad et al. (1999)	8.75	Py100	172.7[c]	3.2[c]	92.0[c]	1.4[c]
Leitner et al. (1980)	0	Py100	177.0 (±1.0)		89.0 (±1.0)	
O'Neill et al. (1991)	0	Py100	172.8 (±0.3)		92.0 (±0.2)	
O'Neill et al. (1991)	0	Py90Alm8Gr2	172.4 (±0.7)		93.2 (±0.5)	
Jiang et al. (2004)	12	Py20Alm72Gr3Sp3And2	174.9 (±1.6)	4.7 (±0.3)	95.6 (±0.5)	1.4 (±0.1)
Ultrasonic interferometry						
Chen et al. (1999)	10	Py100	171.0 (±2.0)	5.3 (±0.4)	92.0 (±1.0)	1.6 (±0.2)
Gwanmesia et al. (2006)	8.7	Py100	175.0 (±2.0)	3.9 (±0.3)	91.0 (±1.0)	1.7 (±0.2)
Gwanmesia et al. (2007)	0.3	Py100	166.0 (±0.2)		92.2 (±1.0)	
Chen et al. (1997)	0	Py98Alm2	173.0[c]		92[c]	
Wang and Ji (2001)	3	Py94Alm6	170.1 (±1.1)	4.9 (±0.6)	90.2 (±0.7)	2.1 (±0.2)
Bonczar et al. (1977)	1	Py61Alm36Gr2	168.2 (±0.4)	4.7 (±0.2)		
Webb (1989)	3	Py61Alm36Gr2	173.6 (±0.4)	4.9 (±0.1)	94.9[c]	1.56[c]
Chen et al. (1997)	0	Py27Alm73	175.0[c]		99.0[c]	
Soga (1967)	0.3	Py21Alm76Gr3	177.0[c]	5.4[c]	94.3[c]	1.4[c]
Verma (1960)	0	Py14Alm81Ca4Sp1	176.5[c]		95.1[c]	
Wang and Ji (2001)	3	Alm100	175.1 (±0.9)	6.2 (±0.5)	92.1 (±0.5)	1.6 (±0.2)

[a] Only Brillouin scattering and ultrasonic interferometry results are listed for pyrope–almandine garnets.
[b] Py: pyrope, $Mg_3Al_2Si_3O_{12}$; Alm: almandine, $Fe_3Al_2Si_3O_{12}$; Gr: grossular, $Ca_3Al_2Si_3O_{12}$; Sp: spessartine, $Mn_3Al_2Si_3O_{12}$; And: $Ca_3Fe_2Si_3O_{12}$.
[c] The uncertainty is not available in the text.

Table 3
Bulk and shear moduli and their temperature derivatives of the pyrope–almandine garnets.[a]

Study	Composition[b]	K_{S0} (GPa)	$(\partial K_S/\partial T)_P$ (MPa/K)	K_{T0} (GPa)	$(\partial K_T/\partial T)_P$ (MPa/K)	G_0 (GPa)	$(\partial G/\partial T)_P$ (MPa/K)
Brillouin scattering							
This study (revised)	Py68Alm24Gr5Sp1	168.2 (±1.8)	−16.8 (±1.3)	167.0 (±1.8)	−23.5 (±2.0)	92.1 (±1.1)	−5.1 (±1.1)
This study (linear)	Py68Alm24Gr5Sp1	169.9 (±1.5)	−16.5 (±2.0)	168.7 (±1.5)	−23.3 (±4.0)	93.2 (±0.6)	−3.6 (±1.4)
Sinogeikin and Bass (2002)	Py100	171.0 (±2.0)	−14.0 (±2.0)	169.4 (±2.0)	−19.4 (±3.0)	94.0 (±2.0)	−9.2 (±1.0)
Ultrasonic interferometry							
Gwanmesia et al. (2006)	Py100	175.0 (±2.0)	−18.0 (±2.0)	172.0 (±2.0)	−26.0 (±4.0)	91.0 (±1.0)	−10.0 (±1.0)
Gwanmesia et al. (2007)	Py100	166.0 (±0.2)	−19.3 (±0.4)	164.3[d]	−26.0[d]	92.2 (±1.0)	−10.4 (±0.2)
Suzuki and Anderson (1983)	Py73Alm16And4Uv6	171.2 (±0.8)	−19.4[c]	169.4[d]	−25.6[c]	92.6 (±0.3)	−10.2[c]
Sumino and Nishizawa (1978)	Py73Alm16And4Uv6	171.2 (±1.6)	−22.5 (±1.2)			92.7 (±0.1)	−8.7 (±0.3)
Bonczar et al. (1977)	Py62Alm36	168.2 (±0.4)	−18.8 (±0.6)				
Sumino and Nishizawa (1978)	Py50Alm46Gr2And1	173.6 (±1.6)	−22.7 (±2.5)			95.3 (±0.1)	−10.7 (±0.3)
Sumino and Nishizawa (1978)	Py39Alm54Gr5And1	173.5 (±1.2)	−22.7 (±2.3)			95.5 (±0.1)	−10.9 (±0.3)
Soga (1967)	Py21Alm76Gr3	177.0[d]	−20.1[d]			94.3[d]	−10.6[d]

[a] Only Brillouin scattering and ultrasonic interferometry results are listed for pyrope–almandine garnets.
[b] Py: pyrope, $Mg_3Al_2Si_3O_{12}$; Alm: almandine, $Fe_3Al_2Si_3O_{12}$; Gr: grossular, $Ca_3Al_2Si_3O_{12}$; Sp: spessartine, $Mn_3Al_2Si_3O_{12}$; And: $Ca_3Fe_2Si_3O_{12}$; Uv: $Ca_3Cr_2Si_3O_{12}$.
[c] Linear fits to reported data by Sinogeikin and Bass (2002).
[d] The uncertainty is not available in the text.

the Fe effect on elasticity in pyrope and to explain the difference between these studies.

We have also compared the temperature derivatives of the bulk and shear moduli in Fe-bearing pyrope to the literature results (Table 3) (Soga, 1967; Bonczar et al., 1977; Sumino and Nishizawa, 1978; Suzuki and Anderson, 1983; Sinogeikin and Bass, 2002; Gwanmesia et al., 2006, 2007). Our derived $(\partial K_S/\partial T)_P$ for Fe-bearing pyrope is in good agreement with that determined by both Brillouin and ultrasonic methods for pure-pyrope within experimental uncertainties (e.g. Sinogeikin and Bass, 2002; Gwanmesia et al., 2006). We also note that the effect of temperature on the shear modulus $(\partial G/\partial T)_P$ obtained in this study is much smaller than that of previous works (e.g. Sinogeikin and Bass, 2002; Gwanmesia et al., 2006). The $(\partial G/\partial T)_P$ obtained either from the linear fitting or the "revised linear fitting" method are both listed in Table 3. The difference in $(\partial G/\partial T)_P$ between this study and previous works may be partly caused by the tradeoff between G_0, $(\partial G/\partial P)_T$ and $(\partial G/\partial T)_P$ in deriving $(\partial G/\partial T)_P$ from the high P–T measurements. For example, our analyses show that a variation in G_0 by 2% or in $(\partial G/\partial P)_T$ by 15% can result in a 100–200% change in $(\partial G/\partial T)_P$, even though these variations in G_0 or $(\partial G/\partial P)_T$ are still within the experimental uncertainties of the current study, indicating that the precision in these derived parameters are strongly correlated in both linear and revised linear fitting methods. To better constrain $(\partial G/\partial T)_P$, further examinations through high-precision, high P–T experiments on the pyrope–almandine system are needed.

4.2. Implication for the Earth's upper mantle

With our updated single-crystal elasticity data of iron-bearing pyrope, here we have calculated elastic V_P and V_S anisotropies of the major upper-mantle minerals. The region above 200 km was not considered in the calculations here because of the complexity in mineral assemblage, chemical heterogeneity and large seismic

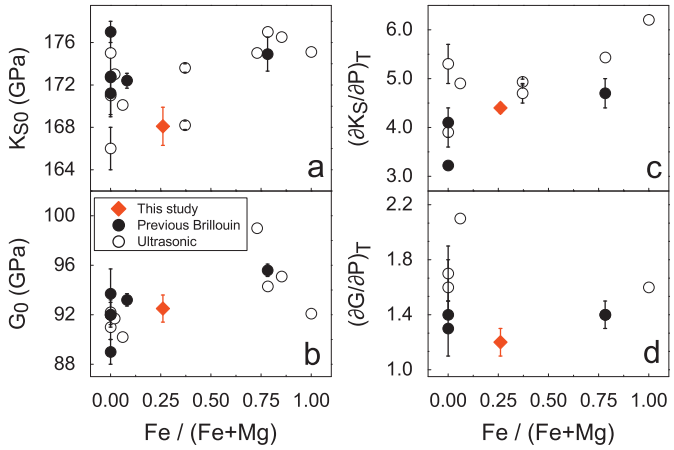

Fig. 4. Bulk and shear moduli and their pressure derivatives in the pyrope–almandine system. (a) Adiabatic bulk modulus (K_{S0}); (b) shear modulus (G_0); (c) pressure derivative of the bulk modulus at 300 K ($(\partial K_S/\partial P)_T$); (d) pressure derivative of the shear modulus at 300 K ($(\partial G/\partial P)_T$). Red diamonds: this study; black filled circles: previous Brillouin scattering results (Leitner et al., 1980; O'Neill et al., 1991; Conrad et al., 1999; Sinogeikin and Bass, 2000; Jiang et al., 2004); open circles: previous ultrasonic results (Verma, 1960; Soga, 1967; Bonczar et al., 1977; Webb, 1989; Chen et al., 1997, 1999; Wang and Ji, 2001; Gwanmesia et al., 2006, 2007). (For interpretation of the references to color in this figure legend, the reader is referred to the web version of this article.)

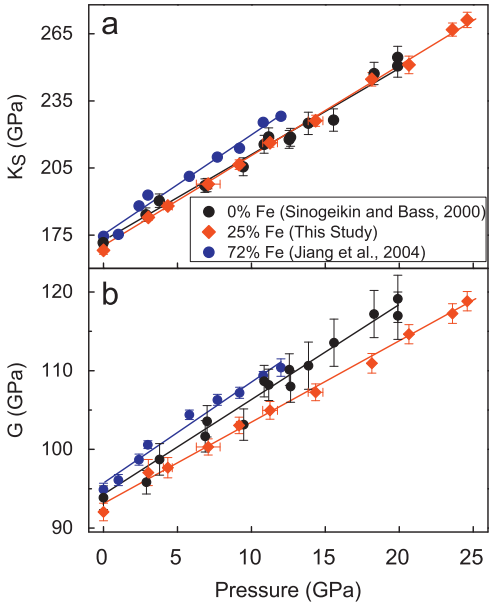

Fig. 5. Comparison of the adiabatic bulk (K_S) and shear (G) moduli in the pyrope–almandine system at high pressure from Brillouin scattering studies. Black circles: pyrope with 25 mol% Fe to 25 GPa (this study); red diamonds: pure pyrope without any Fe to 20 GPa (Sinogeikin and Bass, 2000); blue circles: pyrope with 72 mol% Fe to 11 GPa (Jiang et al., 2004). (For interpretation of the references to color in this figure legend, the reader is referred to the web version of this article.)

heterogeneity (e.g. Jordan, 1975; Grand and Helmberger, 1984). The well-documented existence of low velocity zone above 200 km, for example, requires the results from partial melting study instead of simply using single-crystal elasticity data, which was not the major goal of this study (e.g. Zhao et al., 1992; Webb and Forsyth, 1998). The maximum anisotropy (A) is calculated using single-crystal elasticity of each given mineral following the method in Mainprice et al. (2000):

$$A = 2 \times [(V_{max} - V_{min})/(V_{max} + V_{min})] \times 100\% \quad (16)$$

where V_{max} and V_{min} represent the maximum and minimum V_P or V_S velocity of the mineral, respectively. Literature thermal elastic constants and thermal expansion coefficients used here include Fe-bearing garnet (this study; Fei, 1995), olivine (Isaak, 1992; Abramson et al., 1997; Zha et al., 1998; Liu and Li, 2006), orthopyroxene (Chai et al., 1997; Jackson et al., 2003, 2007), and clinopyroxene (Finger and Ohashi, 1976; Matsui and Busing, 1984; Isaak et al., 2006). These values were further evaluated along a representative upper mantle geotherm (Stacey, 1992) by extrapolating the experimentally measured elastic constants and their P–T derivatives to relevant P–T conditions using the third-order Eulerian finite-strain equation (Birch, 1978):

$$C_{ijkl}(f) = (1+2f)^{7/2}\left(C^T_{ijkl,0} + bf\right) - P\Delta_{ijkl} \quad (17)$$

$$b = 3K^T_{S0}\left(C'^T_{ijkl,0} + \Delta_{ijkl}\right) - 7C^T_{ijkl,0} \quad (18)$$

$$\Delta_{ijkl} = -\delta_{ij}\delta_{kl} - \delta_{ik}\delta_{jl} - \delta_{il}\delta_{jk} \quad (19)$$

where $C^T_{ijkl,0}$ represents each elastic constants at room pressure and a given temperature (T), $C'^T_{ijkl,0}$ is the pressure derivative of the elastic constant, and K^T_{S0} represents the adiabatic bulk modulus at room pressure and a given temperature. Our calculations show that both the shear and compressional anisotropies of the Fe-bearing pyrope are extremely small (within 1% for both compressional and shear waves). In contrast to the very small anisotropies in garnet, olivine and pyroxene exhibit significantly larger anisotropy in the range of 13–43%: olivine exhibits the largest A_{V_P} of ~20–24% and A_{V_S} of ~37–33%, whereas clinopyroxene displays ~13–18% for A_{V_P} and ~32–43% for A_{V_S}, orthopyroxene shows ~13–15% for A_{V_P} and ~21–25% for A_{V_S} (Fig. 6). Due to the extremely small anisotropy of our Fe-bearing pyrope, it is likely that garnet does not play a major role in the seismic anisotropy in the upper mantle region, suggesting that the seismic anisotropy in the upper mantle (200–400 km depth) is mainly caused by the crystal preferred orientation of olivine and pyroxene (Mainprice et al., 2000).

To better understand seismic profiles and mineralogical models of the upper mantle, we have also modeled the V_P and V_S profiles of two representative upper-mantle mineral assemblages, piclogite and pyrolite, using updated elastic properties of Fe-bearing pyrope for the Earth's upper mantle region between 200 and 400 km depth along a normal continental geotherm (Stacey, 1992). The third-order Eulerian finite-strain equation (Eqs. (9) and (10)) (Birch, 1978) and the third-order Birch–Murnaghan

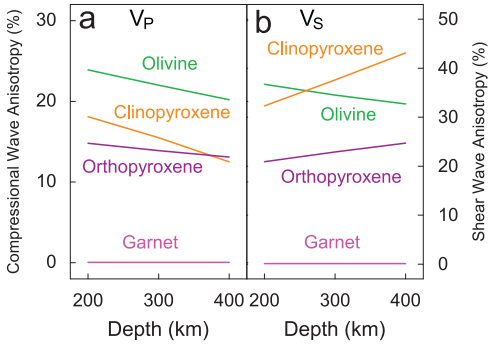

Fig. 6. Compressional (V_P) and shear (V_S) wave anisotropy of major minerals in the upper mantle. The anisotropy factor (A) is defined by $2\times(V_{max}-V_{min})/(V_{max}+V_{min})\times 100\%$ for both V_P and V_S (Mainprice et al., 2000). Magenta lines: garnet, this study; green lines: olivine (Isaak, 1992; Abramson et al., 1997; Zha et al., 1998; Liu and Li, 2006); orange lines: clinopyroxene (Finger and Ohashi, 1976; Matsui and Busing, 1984; Isaak et al., 2006); purple lines: orthopyroxene (Chai et al., 1997; Jackson et al., 2003, 2007). (For interpretation of the references to color in this figure legend, the reader is referred to the web version of this article.)

EoS (Eq. (14)) (Birch, 1978) were used to calculate the K_S, G, V_P, and V_S of the Fe-bearing pyrope at high P–T . Our modeling here is limited to the region between 200 and 400 km depth because of the relatively large regional seismic variations observed above 200 km depth (e.g. Grand and Helmberger, 1984). Compared with the modeled velocities of pure pyrope (Gwanmesia et al., 2006) at the P–T conditions of 200 km depth, our results show that the Fe effect on elasticity of pyrope leads to a ~3% increase in the V_S but negligible change in the V_P within experimental uncertainties. In addition, the V_P and V_S profiles of olivine and pyroxene are also modeled using existing literature results on elasticity and thermodynamic parameters (Finger and Ohashi, 1976; Duffy and Anderson, 1989; Isaak, 1992; Chai et al., 1997; Zha et al., 1998; Jackson et al., 2003, 2007; Liu and Li, 2006; Isaak et al., 2006). We used the Fe/(Fe+Mg) ratio of ~10% for olivine and pyroxene, and ~20% for garnet following the iron partitioning results by Irifune and Isshiki (1998).

Comparison between the modeled V_P and V_S profiles and representative global and regional seismic profiles in the region (Dziewonski and Anderson, 1981; Grand and Helmberger, 1984; LeFevre and Helmberger, 1989; Kennett, 1991; Kennett et al., 1995) shows that the V_P and V_S profiles of garnet are respectively ~5% and ~7% faster than the PREM (Dziewonski and Anderson, 1981) (Fig. 7). On the other hand, the V_S profile of olivine is very close to the seismic model but its V_P profile is slightly lower. Compared with garnet and olivine, the V_P and V_S profiles of pyroxene are ~4–6% and ~1–4% slower than the seismic models, respectively.

We have further evaluated the effects of the volume fractions of these minerals in the pyrolite and piclogite compositional models of the upper mantle (Ringwood, 1975; Anderson and Bass, 1984; Ita and Stixrude, 1992) (Fig. 7). The pyrolite and piclogite models represent two global mineral compositions of the upper mantle that are commonly used for comparison between mineral physics results and global seismic profiles (e.g. Bass and Anderson, 1984; Duffy and Anderson, 1989; Cammarano et al., 2003; Li and Liebermann, 2007). The mineral assemblage in the pyrolite model includes ~63% olivine, ~15% garnet, ~16% clinopyroxene (Cpx), and ~6% orthopyroxene (Opx) (Ita and Stixrude, 1992), whereas the piclogite model includes ~43% olivine, ~15% garnet, ~36% Cpx, and ~6% Opx (Ita and Stixrude, 1992). We note that our modeled velocity profiles only took existing P–T -compositional effects on the elastic velocities into account. In order to build a more robust model, potential effects of anelasticity also need to be considered in the future study (Karato, 1993). Nevertheless, the pyrolite model appears to have slightly greater V_P and V_S velocities than the piclogite model, because of their mineralogical difference (~20% olivine in the pyrolite model is replaced by clinopyroxene in the picolgite model) (Fig. 7). Although the modeled V_S profiles of both pyrolite and piclogite models match well with the seismic profiles, their V_P profiles are approximately 2–5% lower than the PREM and AK135-f models at 300 km depth, together with a small mismatch in the velocity gradient to both PREM and AK135-f models (Dziewonski and Anderson, 1981; Kennett, 1991; Kennett et al., 1995). On the other hand, our modeled V_P profile matches some of the regional seismic models very well (Fig. 7) (LeFevre and Helmberger, 1989), suggesting that an in-depth understanding of the variation between global and regional seismic models is needed to better constrain an existing mineralogical model of the mantle. For a mineralogical model that matches the global seismic observations, the proportion of garnet needs to be much higher because garnet exhibits highest sound velocities among all upper mantle major minerals (Fig. 7). Further simulation in which the mineral contents are allowed to vary indicates that approximately 30% garnet is needed to match the AK135-f seismic model for both V_P and V_S profiles to the pyrolite model when the volume of olivine or pyroxene is fixed. However, such high amount of garnet would significantly affect either Al content or Mg/Si ratio needed in the upper mantle, which needs to be reconciled with the chemical composition of the upper mantle from geochemical study results. It is possible that this mismatch may be simply a result of limited experimental data that have been extrapolated to extreme P–T conditions of the upper mantle, showing the need to measure the elasticity of all major mantle minerals at relevant P–T conditions in the future. Future considerations of factors such as iron partitioning as a function of depth in these minerals (e.g. Irifune and Isshiki, 1998), the anelastic effect (Karato, 1993), and variable temperature gradient (e.g. Brown and Shankland, 1981; Stacey, 1992; Katsura et al., 2010) may also help to reconcile these mismatches.

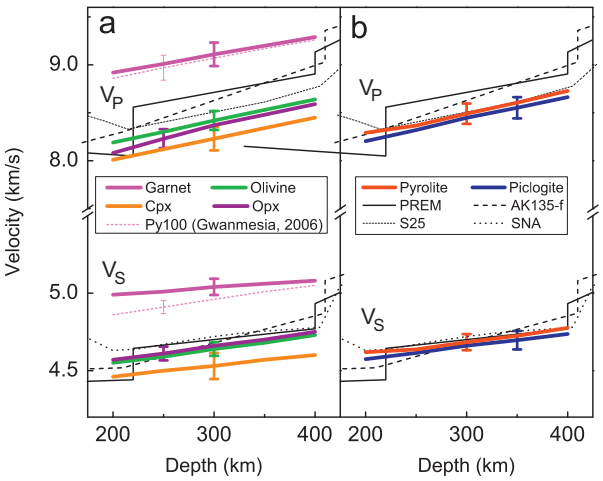

Fig. 7. Modeled velocities of the upper-mantle minerals along a representative geotherm (Stacey, 1992). (a) Sound velocities of major minerals in the upper mantle compared with representative seismological models. Magenta lines: Fe-bearing pyrope (garnet) in this study; green lines: olivine (Isaak, 1992; Zha et al., 1998; Liu and Li, 2006); orange lines: clinopyroxene (Cpx) (Finger and Ohashi, 1976; Duffy and Anderson, 1989; Isaak et al., 2006); purple lines: orthopyroxene (Opx) (Chai et al., 1997; Jackson et al., 2003, 2007). (b) Velocity model in pyrolite (red) and piclogite (blue) composition. Seismic models in (a) and (b) include PREM in black solid lines (Dziewonski and Anderson, 1981), AK135-f in long dash lines (Kennett, 1991; Kennett et al., 1995), S25 in short dash lines (LeFevre and Helmberger, 1989) and SNA in dotted lines (Grand and Helmberger, 1984). (For interpretation of the references to color in this figure legend, the reader is referred to the web version of this article.)

In summary, we have measured the single-crystal elasticity of natural Fe-bearing pyrope, $Mg_{2.04}Fe_{0.74}Ca_{0.16}Mn_{0.05}Al_2Si_3O_{12}$, at simultaneous high P–T conditions up to 20 GPa and 750 K. Compared to literature results, our results indicate that addition of 25 mol% Fe in pyrope can increase the pressure derivative of the bulk modulus by 7% but has negligible effect on the other elastic parameters. Extrapolation of our results to relevant P–T conditions of the upper mantle also shows that Fe-bearing pyrope is almost elastically isotropic in that region, indicating that the seismic anisotropy in the upper mantle may be caused by the crystal preferred orientation and elastic anisotropy of olivine and pyroxene. Using our updated elastic parameters of Fe-bearing pyrope, we have constructed new velocity profiles for representative pyrolite and piclogite models. Our results show that the V_S profiles of both pyrolite and piclogite models are consistent with seismic observations, while V_P profiles are slightly lower than global seismic observations.

Acknowledgments

We thank I. Kantor, J. Liu, J. Wu, J. Yang, P. Dera, Y. Meng, E. Kelly, J. Zhou, and L. Marshall for experimental assistance. We

are also grateful to S. Grand, J. Lassiter, T. Duffy and Y. Wang for their helpful discussion. J.F. Lin acknowledges financial supports from the US National Science Foundation (EAR-0838221, EAR-1053446) and the Carnegie/DOE Alliance Center (CDAC). High *P–T* Brillouin and X-ray diffraction measurements of this study were performed at GeoSoilEnviroCARS (Sector 13), APS, ANL. GeoSoilEnviroCARS is supported by research grants from the Earth Sciences Program of the National Science Foundation (EAR-1128799) and the Geosciences Program of the Department of Energy (DE-FG02-94ER14466). We also thank HPCAT for the use of the ruby and X-ray diffraction systems. HPCAT is supported by CIW, CDAC, UNLV and LLNL through funding from DOE-NNSA , DOE-BES and NSF. APS is supported by DOE-BES, under Contract no. DE-AC02-06CH11357.

References

Abramson, E.H., Brown, J.M., Slutsky, L.J., Zaug, J., 1997. The elastic constants of San Carlos olivine to 17 GPa. J. Geophys. Res. 102, 12253–12263.

Anderson, D.L., Bass, J.D., 1984. Mineralogy and composition of the upper mantle. Geophys. Res. Lett. 11, 637–640.

Ando, M., Ishikawa, Y., Wada, H., 1980. S-wave anisotropy in the upper mantle under a volcanic area in Japan. Nature 286, 43–46.

Bass, J.D., Anderson, D.L., 1984. Composition of the upper mantle: geophysical tests of two petrological models. Geophys. Res. Lett. 11, 229–232.

Birch, F., 1978. Finite strain isotherm and velocities for single-crystal and polycrystalline NaCl at high pressures and 300 K. J. Geophys. Res. 83, 1257–1268.

Bonczar, L.J., Graham, E.K., Wang, H., 1977. The pressure and temperature dependence of the elastic constants of pyrope garnet. J. Geophys. Res. 82, 2529–2534.

Brown, J.M., Shankland, T.J., 1981. Thermodynamic parameters in the Earth as determined from seismic profiles. Geophys. J. R. Astron. Soc. 66, 579–596.

Cammarano, F., Goes, S., Vacher, P., Giardini, D., 2003. Inferring upper-mantle temperatures from seismic velocities. Phys. Earth Planet. Inter. 138, 197–222.

Chai, M., Brown, J.M., Slutsky, L.J., 1997. The elastic constants of an aluminous orthopyroxene to 12.5 GPa. J. Geophys. Res. 102, 14779–14785.

Chen, G., Miletich, R., Mueller, K., Spetzler, H.A., 1997. Shear and compressional mode measurements with GHz ultrasonic interferometry and velocity-composition systematics for the pyrope–almandine solid solution series. Phys. Earth Planet. Inter. 99, 273–287.

Chen, G., Cooke Jr., J.A., Gwanmesia, G.D., Liebermann, R.C., 1999. Elastic wave velocities of $Mg_3Al_2Si_3O_{12}$–pyrope garnet to 10 GPa. Am. Mineral. 84, 384–388.

Conrad, P.G., Zha, C.S., Mao, H.K., Hemley, R.J., 1999. The high-pressure, single-crystal elasticity of pyrope, grossular, and andradite. Am. Mineral. 84, 374–383.

Dai, L., Karato, S., 2009. Electrical conductivity of pyrope-rich garnet at high temperature and high pressure. Phys. Earth Planet. Inter. 176, 83–88.

Duffy, T.S., Anderson, D.L., 1989. Seismic velocities in mantle minerals and mineralogy of the upper mantle. J. Geophys. Res. 94, 1895–1912.

Dziewonski, A.M., Anderson, D.L., 1981. Preliminary reference Earth model. Phys. Earth Planet. Inter. 25, 297–356.

Every, A.G., 1980. General closed-form expressions for acoustic waves in elastically anisotropic solids. Phys. Rev. B 22, 1746–1760.

Fei, Y., 1995. Thermal expansion. In: Ahrens, T.J. (Ed.), Mineral Physics and Crystallography: A Handbook of Physical Constants, AGU Reference Shelf, vol. 2. American Geophysical Union, Washington, DC, pp. 29–44.

Fei, Y., Bertka, C.M., 1999. Phase transitions in the Earth's mantle and mantle mineralogy. In: Fei, Y., Bertka, C.M., Mysen, B.O. (Eds.), Mantle Petrology: Field Observations and High Pressure Experimentation: A Tribute to F.R. Boyd, Geochemical Society Special Publication 6. The Geochemical Society, Houston, TX, pp. 189–207.

Fei, Y., Ricolleau, A., Frank, M., Mibe, K., Shen, G., Prakapenka, V., 2007. Toward an internally consistent pressure scale. Proc. Natl. Acad. Sci. USA 104, 9182–9186.

Finger, L.W., Ohashi, Y., 1976. The thermal expansion of diopside to 800 °C and a refinement of the crystal structure at 700 °C. Am. Mineral. 61, 303–310.

Giesting, P.A., Hofmeister, A.M., 2002. Thermal conductivity of disordered garnets from infrared spectroscopy. Phys. Rev. B 65, 144305.

Gillet, P., Fiquet, G., Malezieux, J.M., Geiger, C.A., 1992. High-pressure and high temperature Raman spectroscopy of end-member garnets: pyrope, grossular and andradite. Eur. J. Mineral. 4, 651–664.

Grand, S.P., Helmberger, D.V., 1984. Upper mantle shear structure of North America. Geophys. J. R. Astron. Soc. 76, 399–438.

Gwanmesia, G.D., Zhang, J., Darling, K., Kung, J., Li, B., Wang, L., Neuville, D., Liebermann, R.C., 2006. Elasticity of polycrystalline pyrope ($Mg_3Al_2Si_3O_{12}$) to 9 GPa and 1000 °C. Phys. Earth Planet. Inter. 155, 179–190.

Gwanmesia, G.D., Jackson, I., Liebermann, R.C., 2007. In search of the mixed derivative $\partial^2 M/\partial P\partial T$ ($M=G$, K): joint analysis of ultrasonic data for polycrystalline pyrope from gas- and solid-medium apparatus. Phys. Chem. Miner. 34, 85–93.

Hess, H.H., 1964. Seismic anisotropy of the uppermost mantle under oceans. Nature 203, 629–631.

Hill, R., 1952. The elastic behaviour of a crystalline aggregate. Proc. Phys. Soc. A 65, 349–354.

Irifune, T., Isshiki, M., 1998. Iron partitioning in a pyrolite mantle and the nature of the 410-km seismic discontinuity. Nature 392, 702–705.

Irifune, T., Higo, Y., Inoue, T., Kono, Y., Ohfuji, H., Funakoshi, K., 2008. Sound velocities of majorite garnet and the composition of the mantle transition region. Nature 451, 814–817.

Isaak, D.G., 1992. High-temperature elasticity of iron-bearing olivines. J. Geophys. Res. 97, 1871–1885.

Isaak, D.G., Ohno, I., Lee, P.C., 2006. The elastic constants of monoclinic single-crystal chrome-diopside to 1300 K. Phys. Chem. Miner. 32, 691–699.

Ita, J., Stixrude, L., 1992. Petrology, elasticity, and composition of the mantle transition zone. J. Geophys. Res. 97, 6849–6866.

Jackson, J.M., Palko, J.W., Andrault, D., Sinogeikin, S.V., Lakshtanov, D.L., Wang, J., Bass, J.D., Zha, C.-S., 2003. Thermal expansion of natural orthoenstatite to 1473 K. Eur. J. Mineral. 15, 469–473.

Jackson, J.M., Sinogeikin, S.V., Bass, J.D., 2007. Sound velocities and single-crystal elasticity of orthoenstatite to 1073 K at ambient pressure. Phys. Earth Planet. Inter. 161, 1–12.

Jacobsen, S.D., Reichmann, H.-J., Spetzler, H.A., Mackwell, S.J., Smyth, J.R., Angel, R.J., McCammon, C.A., 2002. Structure and elasticity of single-crystal (Mg,Fe)O and a new method of generating shear waves for gigahertz ultrasonic interferometry. J. Geophys. Res. 107, B22037.

Jiang, F., Speziale, S., Duffy, T.S., 2004. Single-crystal elasticity of grossular- and almandine-rich garnets to 11 GPa by Brillouin scattering. J. Geophys. Res. 109, B10210.

Jordan, T.H., 1975. Lateral heterogeneity and mantle dynamics. Nature 257, 745–750.

Kanamori, H., Fujii, N., Mizutani, H., 1968. Thermal diffusivity measurement of rock-forming minerals from 300° to 1100 °K. J. Geophys. Res. 73, 595–605.

Karato, S., 1993. Importance of anelasticity in the interpretation of seismic tomography. Geophys. Res. Lett. 20, 1623–1626.

Katsura, T., Yoneda, A., Yamazaki, D., Yoshino, T., Ito, E., 2010. Adiabatic temperature profile in the mantle. Phys. Earth Planet. Inter. 183, 212–218.

Kawasaki, I., Konno, F., 1984. Azimuthal anisotropy of surface-waves and the possible type of the seismic anisotropy due to preferred orientation of olivine in the uppermost mantle beneath the Pacific-ocean. J. Phys. Earth 32, 229–244.

Kennett, B.L.N., 1991. Seismic velocity gradients in the upper mantle. Geophys. Res. Lett. 18, 1115–1118.

Kennett, B.L.N., Engdahl, E.R., Buland, R., 1995. Constraints on seismic velocities in the Earth from traveltimes. Geophys. J. Int. 122, 108–124.

Lee, C.-T.A., 2003. Compositional variation of density and seismic velocities in natural peridotites at STP conditions: implications for seismic imaging of compositional heterogeneities in the upper mantle. J. Geophys. Res. 108, 2441–2461.

LeFevre, L.V., Helmberger, D.V., 1989. Upper mantle *P* velocity structure of the Canadian Shield. J. Geophys. Res. 94, 17749–17765.

Leitner, B.J., Weidner, D.J., Liebermann, R.C., 1980. Elasticity of single crystal pyrope and implications for garnet solid solution series. Phys. Earth Planet. Inter. 22, 111–121.

Li, B., Liebermann, R.C., 2007. Indoor seismology by probing the Earth's interior by using sound velocity measurements at high pressures and temperature. Proc. Natl. Acad. Sci. USA 104, 9145–9150.

Liu, W., Li, B., 2006. Thermal equation of state of $(Mg_{0.9}Fe_{0.1})_2SiO_4$ olivine. Phys. Earth Planet. Inter. 157, 188–195.

Mainprice, D., Barruol, G., Ismail, W.B., 2000. The seismic anisotropy of the Earth's mantle: from single crystal to polycrystal. In: Karato, S., et al. (Eds.), Earth's Deep Interior: Mineral Physics and Tomography from the Atomic to the Global Scale, Geophysical Monograph Series, vol. 117. American Geophysical Union, Washington, DC.

Mao, H.K., Xu, J., Bell, P.M., 1986. Calibration of the ruby pressure gauge to 800 kbar under quasi-hydrostatic conditions. J. Geophys. Res. 91, 4673–4676.

Mao, Z., Lin, J.F., Jacobsen, S.D., Duffy, T.S., Chang, Y.Y., Smyth, J.R., Frost, D.J., Hauri, E.H., Prakapenka, V.B., 2012. Sound velocities of hydrous ringwoodite to 16 GPa and 673 K. Earth Planet. Sci. Lett. 331–332, 112–119.

Matsui, M., Busing, W.R., 1984. Calculation of the elastic constants and high-pressure properties of diopside, $CaMgSi_2O_6$. Am. Mineral. 69, 1090–1095.

Montagner, J.-P., Tanimoto, T., 1990. Global anisotropy in the upper mantle inferred from the regionalization of phase velocities. J. Geophys. Res. 95, 4797–4819.

Montagner, J.-P., Kennett, B.L.N., 1996. How to reconcile body-wave and normal-mode reference earth models? Geophys. J. Int. 125, 229–248.

O'Neill, B., Bass, J.D., Rossman, G.R., Geiger, C.A., Langer, K., 1991. Elastic properties of pyrope. Phys. Chem. Miner. 17, 617–621.

Ostwald, J., Pazold, W., Weis, O., 1977. High-resolution Brillouin spectroscopy of water. Appl. Phys. 13, 351–356.

Poli, S., 1993. The amphibolite–eclogite transformation: an experimental study on basalt. Am. J. Sci. 293, 1061–1107.

Polian, A., Vo-Thanh, Dung, Richet, P., 2002. Elastic properites of a-SiO_2 up to 2300 K from Brillouin scattering measurements. Europhys. Lett. 57, 375–381.

Raitt, R.W., Shor Jr., G.G., Francis, T.J.G., Morris, G.B., 1969. Anisotropy of the Pacific upper mantle. J. Geophys. Res. 74, 3095–3190.

Rickwood, P.C., Mathias, M., Siebert, J.C., 1968. A study of garnets from eclogite and peridotite xenoliths found in kimberlite. Contrib. Mineral. Petrol. 19, 271–301.
Ringwood, A.E., 1967. The pyroxene–garnet transformation in the Earth's mantle. Earth Planet. Sci. Lett. 2, 255–263.
Ringwood, A.E., 1975. Composition and Petrology of the Earth's Mantle. McGraw-Hill, New York.
Ringwood, A.E., 1991. Phase transformations and their bearing on the constitution and dynamics of the mantle. Geochim. Cosmochim. Acta 55 (8), 2083–2110.
Romano, C., Poe, B.T., Kreidie, N., McCammon, C.A., 2006. Electrical conductivities of pyrope–almandine garnets up to 19 GPa and 1700 °C. Am. Mineral. 91, 1371–1377.
Silver, P.G., Chan, W.W., 1991. Shear wave splitting and subcontinental mantle deformation. J. Geophys. Res. 96, 16429–16454.
Sinogeikin, S.V., Bass, J.D., 2000. Single-crystal elasticity of pyrope and MgO to 20 GPa by Brillouin scattering in the diamond cell. Phys. Earth Planet. Inter. 120, 43–62.
Sinogeikin, S.V., Bass, J.D., 2002. Elasticity of pyrope and majorite–pyrope solid solutions to high temperatures. Earth Planet. Sci. Lett. 203, 549–555.
Sinogeikin, S.V., Bass, J.D., Prakapenka, V.B., Lakshtanov, D., Shen, G., Sanchez-Valle, C., Rivers, M., 2006. Brillouin spectrometer interfaced with synchrotron radiation for simultaneous x-ray density and acoustic velocity measurements. Rev. Sci. Instrum. 77, 103905.
Soga, N., 1967. Elastic constants of garnet under pressure and temperature. J. Geophys. Res. 72, 4227–4234.
Stacey, F.D., 1992. Physics of the Earth, third edition. Brookfield Press, Brisbane, Qld., Australia.
Sumino, Y., Nishizawa, O., 1978. Temperature variation of elastic constants of pyrope–almandine garnets. J. Phys. Earth 26, 239–252.
Suzuki, I., Anderson, O.L., 1983. Elasticity and thermal expansion of a natural garnet up to 1000 K. J. Phys. Earth 31, 125–138.
Verma, R.K., 1960. Elasticity of some high-density crystals. J. Geophys. Res. 65, 757–766.
Wang, Z., Ji, S., 2001. Elasticity of six polycrystalline silicate garnets at pressure up to 3.0 GPa. Am. Mineral. 86, 1209–1218.
Webb, S.C., Forsyth, D.W., 1998. Structure of the upper mantle under the EPR from waveform inversion of regional events. Science 280, 1227–1229.
Webb, S.L., 1989. The elasticity of the upper mantle orthosilicates olivine and garnet to 3 GPa. Phys. Chem. Miner. 16, 684–692.
Zha, C.-S., Duffy, T.S., Downs, R.T., Mao, H.K., Hemley, R.J., 1998. Brillouin scattering and X-ray diffraction of San Carlos olivine: direct pressure determination to 32 GPa. Earth Planet. Sci. Lett. 159, 25–33.
Zhao, D., Hasegawa, A., Horiuchi, S., 1992. Tomographic imaging of *P* and *S* wave velocity structure beneath northeastern Japan. J. Geophys. Res. 97 (B13), 19909–19928.